

Article

# Certainty Factor Analyses and Spatiotemporal Characteristics of Landslide Evolution: Case Studies in the Chishan River Watershed in Taiwan

Chunhung Wu

Department of Water Resources Engineering and Conservation, Feng Chia University, Taichung 40724, Taiwan; chhuwu@fcu.edu.tw

**Abstract:** The 1999 Chichi earthquake and Typhoon Morakot in 2009 caused two serious landslide events in the Chishan river watershed in southern Taiwan. In this study, certainty factor analysis was used to evaluate the effectiveness of landslide occurrence, and spatiotemporal hotspot analysis was used to explain the pattern and distribution of landslide hotspots. The *Z*-values from the Getis–Ord formula were used to assess the clustering strength of landslide evolution on different scales and with different landslide sizes in different time periods. The landslide-prone area had an elevation of 1000–1750 m, a slope of  $>40^\circ$ , and hillslopes with N, NE, E, and SE aspects and was within 100 m of rivers. The main spatiotemporal hotspot patterns of landslide evolution during 1999–2017 were oscillating hotspots, intensifying hotspots, and persistent hotspots, and the three main hotspot patterns occupied 80.1–89.4% of all hotspot areas. The main spatiotemporal landslide hotspots were concentrated in the core landslide areas and the downslopes of riverbank landslide areas, especially in the upstream subwatersheds. The landslide clustered strength in the upstream watershed was 3.4 times larger than that in the Chishan river watershed, and that in large landslides was 2.4 and 6.6 times larger than those in medium and small landslides, respectively.

**Keywords:** landslide evolution; landslide recovery; spatiotemporal hotspot; certainty factor analysis



**Citation:** Wu, C. Certainty Factor Analyses and Spatiotemporal Characteristics of Landslide Evolution: Case Studies in the Chishan River Watershed in Taiwan. *ISPRS Int. J. Geo-Inf.* **2022**, *11*, 382. <https://doi.org/10.3390/ijgi11070382>

Academic Editors: Walter Chen and Fuan Tsai

Received: 30 April 2022

Accepted: 8 July 2022

Published: 10 July 2022

**Publisher's Note:** MDPI stays neutral with regard to jurisdictional claims in published maps and institutional affiliations.



**Copyright:** © 2022 by the author. Licensee MDPI, Basel, Switzerland. This article is an open access article distributed under the terms and conditions of the Creative Commons Attribution (CC BY) license (<https://creativecommons.org/licenses/by/4.0/>).

## 1. Introduction

Extreme rainfall and large earthquake events have caused severe landslides in several countries; examples of such events include the 1999 Chichi earthquake in Taiwan [1], the 2005 Kashmir earthquake in Pakistan [2,3], the 2008 Wenchuan earthquake in China [4–6], Typhoon Morakot in 2009 in Taiwan [7,8], the 2015 Gorkha earthquake in Nepal [9], and the 2017 Jiuzhaigou earthquake in China [10]. Consequently, the areas affected by such events have become fragile and susceptible to landslides in subsequent years. The landslide susceptibility of mountainous areas after extreme rainfall or large earthquakes changes with time and space. Watersheds that experience numerous earthquake- or extreme-rainfall-induced landslides usually require more than 10 years to recover from such landslides. Moreover, sediment generated by continuous landslides in fragile watersheds is transported to rivers and dominates the subsequent geomorphologic evolution of these rivers. The unstable sediment yield from numerous landslides induced by large earthquake or extreme rainfall events in mountainous regions can cause further sediment disasters in the following years [7,8,11].

Research on post-extreme rainfall and postearthquake landslide evolution is essential for disaster prevention and reduction [4–8]. Accordingly, the spatiotemporal characteristics of landslide evolution and the dominant factors affecting it must be determined to ensure effective watershed management in the years after severe landslide events. Several studies have analyzed the relationship between geomorphological factors—including elevation, slope, aspect, and distance to river—and annual landslide distributions in subsequent years to determine the dominant factors influencing landslide evolution [4,5] and determine

the sensitivity of geomorphological factors affecting landslide occurrence [6]. Because of numerous landslides distributed in the mountainous regions, the thresholds of rainfall for triggering the debris flows in southern Taiwan sharply decreased [7,8]. Furthermore, the distribution and concentration of landslides in the years that follow extreme-rainfall- and large-earthquake-induced landslide events must be compared. Some spatial differences in the distribution of landslide evolution before and after large-earthquake- and extreme-rainfall-induced landslide events have been found [4,7,8]. In the years that follow large earthquake-induced landslide events, the subsequent landslides that occur are typically concentrated in areas with elevations of <2000 m, slopes of 30–50°, aspects identical to the thrust directions of earthquake-induced faults, and slope toes located near rivers [2,4,6]. Nevertheless, few studies have discussed the distribution and concentration of landslides in the years following extreme-rainfall-induced landslide events [12,13]. Landslide recovery time after large earthquake and extreme rainfall events is a key factor for watershed management and has been assessed by several methods. The landslide recovery time was estimated as 2 years by assessing the landslide activity after the 2005 Kashmir earthquake in northern Pakistan [2]; 3–4 years by observing the number and area of annual landslides after the 2008 Wenchuan earthquake in Sichuan, China [5,14]; and 5 years by assessing the ratios of the annual decline in landslide area after Typhoon Morakot in 2009 in southern Taiwan [7,8].

The emerging hotspot analysis technique for spatiotemporal analysis has been used by several scholars to investigate the transmission of the COVID-19 virus [15–17], explore temporal changes in the volume of capture fisheries [18], investigate the distribution of traffic accidents [19,20], track pollutant emissions [21], and analyze the relationship between urban growth and urban fire [22]. Moreover, this new technique has been used to explain the patterns and characteristics of the long-term landslide evolution after extreme-rainfall-induced landslide events in Taiwan [12,13]. Spatiotemporal analysis has been used to explore the spatiotemporal distribution of landslide hotspots [12] and analyze differences in landslide spatiotemporal distribution based on different bin sizes [13] in the landslide-prone watersheds in southern Taiwan. The traditional hotspot analysis approach considers the spatial distribution and clustering of landslides by using a specific time database; by contrast, the emerging hotspot analysis technique can consider the spatial distribution and clustering of landslides by using multiple time databases. The new technique can provide spatiotemporal plots of landslide hotspots, which can be used to explain changes in the spatial patterns and distributions of landslides over time. Accordingly, the spatiotemporal distribution of landslide clustering can be used to explain landslide recovery and watershed evolution in the years that follow severe landslide events.

Southwestern Taiwan experienced substantial rainfall during Typhoon Morakot in 2009. Consequently, severe landslides, including the well-known Xiaolin landslide, occurred in the Chishan river watershed [7,8]. The sediment yield induced by this typhoon in the Chishan river watershed was estimated to exceed  $10^8$  m<sup>3</sup> [23]. Therefore, this study investigated the effect of the typhoon-induced sediment yield on watershed evolution in the years that followed Typhoon Morakot. The spatial and temporal changes in landslide clustering intensity in the landslide-prone watershed have never been discussed. This study focused on explaining the spatial and temporal changes in landslide clustering intensity in the landslide-prone watershed in Taiwan by using spatiotemporal analysis and the Z-score of the Getis–Ord formula. The study also compared the landslide recovery after the 1999 Chichi earthquake ( $M_L = 7.2$ ) with that after Typhoon Morakot in 2009 in the Chishan river watershed to determine the differences between and characteristics of the recovery processes after earthquake- and rainfall-induced landslides. The long-term observation of the evolution of landslides in the Chishan river watershed could provide valuable insights for understanding landslide recovery and evolution in southern Taiwan.

## 2. Research Area

The study area was the Chishan river watershed in southwestern Taiwan and covered an area of 612.8 km<sup>2</sup> (Figure 1). The elevation in the study area ranged from 40 to 3950 m above sea level, and the area with elevation <1000 m occupied 51.9% of the study area. The slope in the study area ranged from 0 to 85°, and more than 79.3% of the total study area had a slope <40°. Around 88.2% of the study area was covered by natural forest and agriculture. The Chishan river was the main river in the study area, and its average discharge was 30.1 m<sup>3</sup>/day. The study area was surrounded by 11 faults (Figure 2), including 2 faults passing through the C10 watershed (Figure 1) and 9 faults passing through the C01 to C06 subwatersheds (Figure 1). The lithology in the study area was characterized by sandstone, shale, clay, slate, and interlayered sandstone and shale from the mid-Miocene to the Holocene. The weak geological formations in the study area lead to poor lithologic resistance to landslides and erosion, and the decadal erosion rate was estimated to be around 30 mm/year [24]. The mean suspended-sediment concentration measured at the Shanlin bridge in the downstream of the Chishan river watershed was 696 ppm, and the annual sediment yield was estimated to be around 1.06 Mt/year [24].

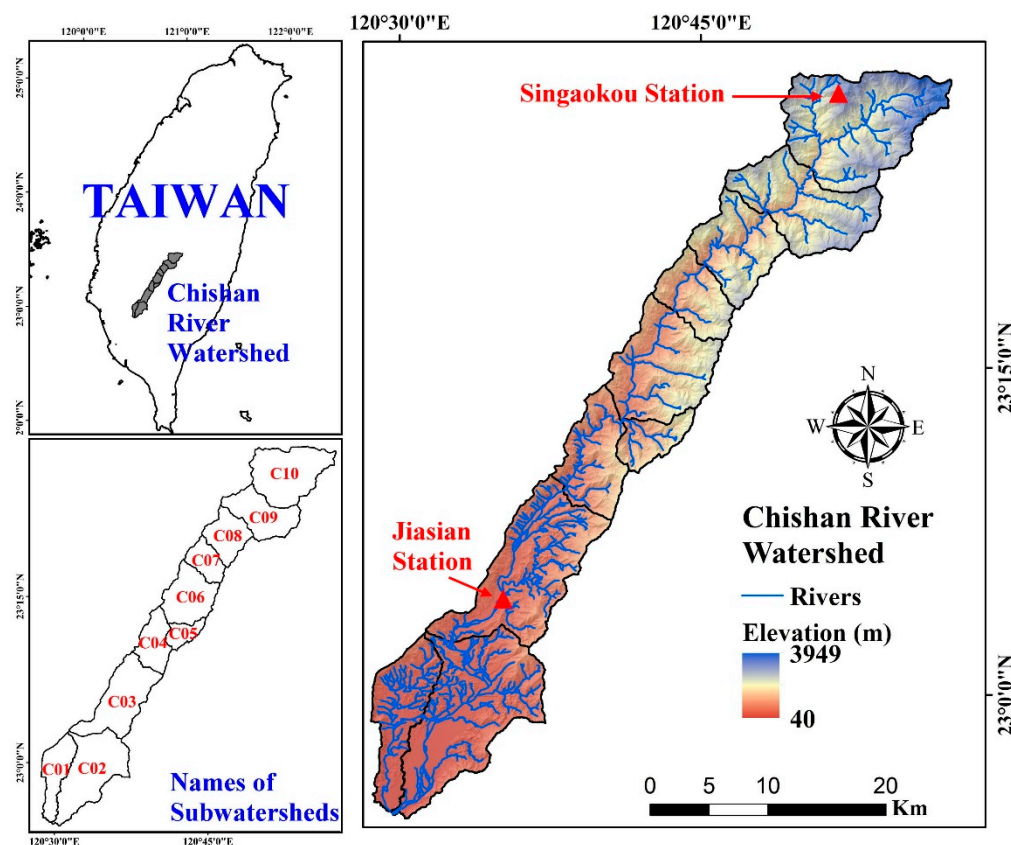


**Figure 1.** The distributions of elevation, rivers (main plot), and subwatersheds (left-down plot) in the Chishan river watershed.

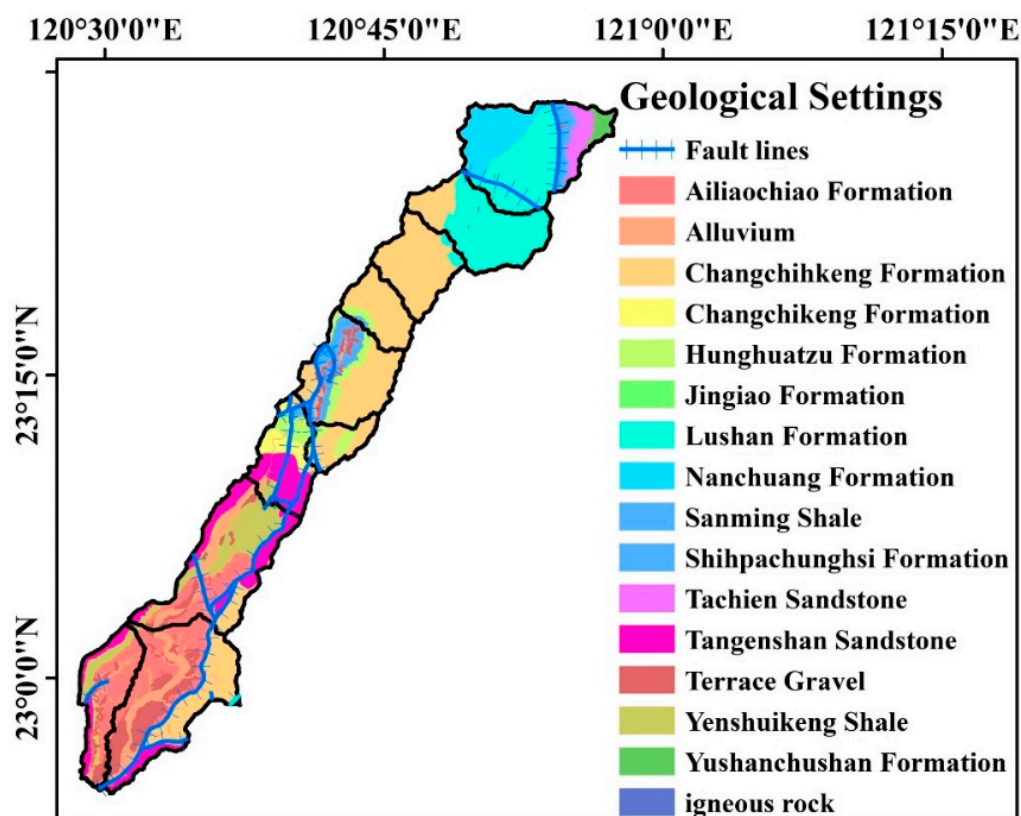


**Figure 2.** The geological settings in the Chishan river watershed.

The average annual rainfall at the Jiasian (low altitude, Figure 1) and Singaokou rainfall stations (high altitude, Figure 1) was around 2845 mm in 1951–2020 and 2908 mm in 1983–2020. The accumulated rainfall in the rainy season (from May to October) occupied >80% of the annual rainfall in the Chishan river watershed [18], and the heavy rainfall and typhoon events from June to September were the main reasons why. The Chishan river watershed is prone to natural disasters (e.g., floods, soil erosion, landslides, and debris flow). The two main geohazards in the Chishan river watershed are landslides and debris flow, and the main landslide-trigger event in 1999–2017 was Typhoon Morakot in 2009. Typhoon Morakot dumped record-breaking rainfall, over 2000 mm in 4 days, and caused very serious landslide disaster events in the Chishan river watershed [7]. As of 2021, the ratio and severity of extreme-rainfall-triggered landsliding from Typhoon Morakot in southern Taiwan were historical highs. Based on the rainfall record of the Jiasian rainfall station, the accumulated rainfall during Typhoon Morakot was 2142 mm, 72.3% of the annual rainfall in 2009. During Typhoon Morakot, there was 31.5 km<sup>2</sup> of landslide area, including 3.8 km<sup>2</sup> and 12.3 km<sup>2</sup> located in the upslope and downslope, respectively, in the Chishan river watershed, and the landslide ratio was estimated to be larger than 7.0% [7]. There were also 39 potential debris flow torrents in the Chishan river watershed in 2021.

### 3. Materials and Methods

#### 3.1. Materials

This study selected the Jiasian and Singaokou rainfall stations (Figure 1) as the representative stations in the Chishan river watershed. The study used rainfall records collected at these two stations for the 1999–2017 period to analyze rainfall characteristics in the study area. The Central Geological Survey and Forestry Bureau of Taiwan provided annual landslide inventories during 1999–2017 in the Chishan river watershed. From these inventories, landslides that occurred during 1999–2002 were identified from SPOT 1 and 2 images with spatial resolutions of 10 m, and those that occurred during 2003–2017 were identified from Formosat-2 images with spatial resolutions of 2 m. The annual landslide inventories during

1999–2002 in Taiwan were produced by using supervised classification to delineate the landslide polygons, and those during 2003–2017 were produced by using the Formosat-2 automatic image processing system [25] and the Expert Landslide and Shaded Area Delineation System (ELSADS) [26] to delineate the landslide polygons. The Formosat-2 imagery during 2003–2017 was preprocessed by using the Formosat-2 automatic image processing system [25]. The Formosat-2 automatic image processing system was able to conduct band-to-band coregistration [25], automatic orthorectification [26], and multitemporal image geometrical registration [27], and it was the main system for producing the annual landslide inventories during 2003–2017 in Taiwan. The Expert Landslide and Shaded Area Delineation System (ELSADS) was used to delineate the polygons of landslides [28]. The landslide distribution maps during 1999–2017 and the landslide susceptibility maps after Typhoon Morakot in 2009 [23] are shown in Figure 3. The landslide cases were classified into three types for further analysis: large (area > 100,000 m<sup>2</sup>), medium (area = 10,000–100,000 m<sup>2</sup>), and small (area < 10,000 m<sup>2</sup>) landslides. The study used a digital elevation model (DEM) with a spatial resolution of 5 m; moreover, a 5 m × 5 m grid was used as the unit of analysis. The study area was classified into 10 subwatersheds (C01–C10, as shown in Figure 1, lower left panel) on the basis of the delineation of subwatersheds in Taiwan.

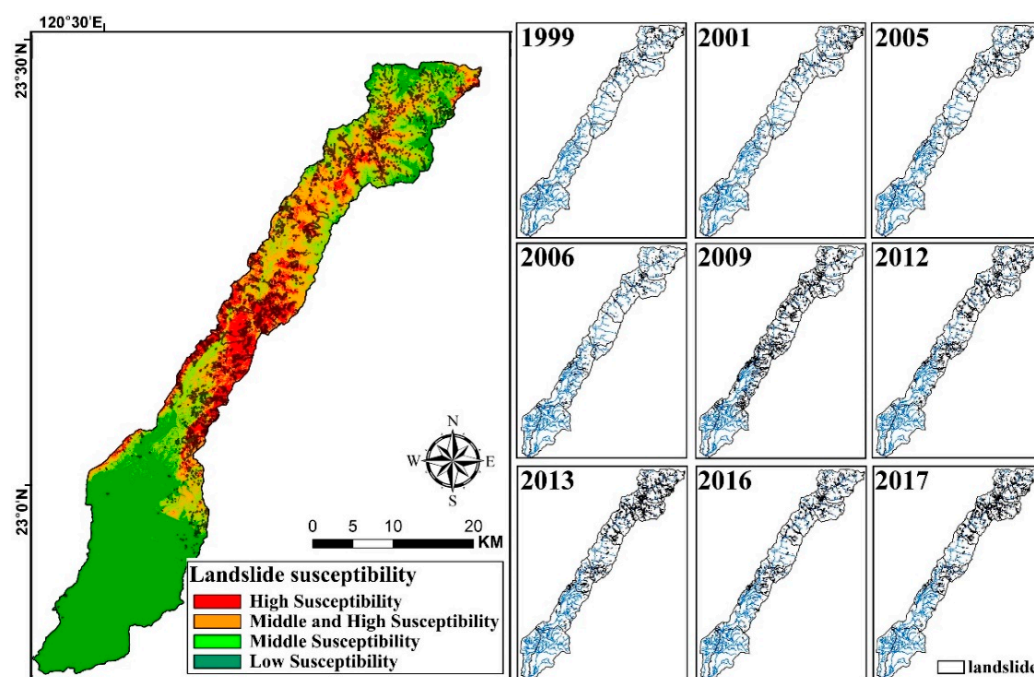


**Figure 3.** The landslide distribution during 1999–2017 (right figures) and the landslide susceptibility map (left figure) in the Chishan river watershed.

### 3.2. Certainty Factor Analyses

A certainty factor analysis and an effectiveness index were used to evaluate the effectiveness of factors on landslide occurrence in the study area. The certainty factor [29,30] can be used to analyze the effectiveness of different factors on the occurrence of events. This study used a certainty factor to identify the main factors influencing landslide occurrence and evolution after the 2008 Wenchuan earthquake in China [6,31]. The present study adapted the following certainty factor [32] for analysis:

$$CF = \frac{P_a - P_s}{P_a \times (1 - P_s)} \text{ if } P_a \geq P_s; \frac{P_a - P_s}{P_s \times (1 - P_a)} \text{ if } P_a < P_s \quad (1)$$

where CF denotes the certainty factor,  $P_a$  denotes the ratio of the landslide area within a subcategory of a factor category to the landslide area in the factor category, and  $P_s$  denotes the ratio of the landslide area to the watershed area. The certainty factor value ranges from

−1 to 1, with positive and negative values indicating increasing and decreasing certainty of landslide occurrence.

This study also used an effectiveness index ( $E$ ) to compare the effectiveness of various factors on landslide occurrence. The effectiveness index ( $E$ ) can be defined as the difference between the maximum and minimum values of the certainty factor and can be used to quantify the influence of each factor on landslide occurrence and evolution.

### 3.3. Local Outlier Analysis

The study used the Anselin local Moran's  $I$  index [33] to analyze the clusters and outliers of landslide evolution in the Chishan river watershed. The Anselin local Moran's  $I$  index was used to identify local clusters and outliers of landslide in the space and time dimensions. Six kinds of patterns were defined: high–high cluster (HH), only high–low outlier (HL), only low–high outlier (LH), only low–low cluster (LL), multiple types (Mul.), and never significant (NS) based on the results of Anselin local Moran's  $I$  index. The low–low (LL) pattern revealed the bins that, along with their neighborhoods, had low landslide ratios or obvious landslide outliers, while the high–high (HH) pattern revealed the bins that, along with their neighborhoods, had high landslide ratios or obvious landslide clusters.

### 3.4. Spatiotemporal Hotspot Analysis

This study mainly used the Getis–Ord formula [34] and the emerging hotspot analysis technique to analyze the spatiotemporal trends of landslide evolution in the Chishan river watershed. The annual landslide inventories for the Chishan river watershed during 1999–2017 were used to establish a space–time cube model. Moreover, the annual landslide inventories during 1999–2008 were used to establish a space–time cube model to analyze the long-term evolution of landslides induced by the 1999 Chichi earthquake; this model comprised 797,912 bins. The annual landslide inventories during 2008–2017 were used to establish a space–time cube model to analyze the long-term evolution of landslides induced by Typhoon Morakot in 2009; this model comprised 1,946,705 bins. In each of these models, a bin represented a  $5\text{ m} \times 5\text{ m}$  grid that had been identified as landslide during 1999–2017. The  $x$ - and  $y$ -axes in the space–time cube model represented the longitude and latitude coordinate information of the bins, and the  $z$ -axis represented the years in which the bins were identified as being affected by landslides.

The Getis–Ord formula was used to explain the distribution of landslide clustering intensity and statistical significance, and the emerging hotspot analysis technique was used to analyze the spatiotemporal distribution and pattern of landslide hotspots. A  $Z$ -score was derived using the Getis–Ord formula; this measure indicated the strength and statistical significance of landslide clustering hotspots and cold spots (Table 1).

**Table 1.** Classification and statistical significance of hotspot and cold spots based on  $Z$ -scores.

Z-Score	Hotspot or Cold Spot	Confidence Level
>2.58	Hotspot	99% confidence level
1.96–2.58	Hotspot	95% confidence level
1.65–1.96	Hotspot	90% confidence level
−1.65–1.65	No statistical significance	
−1.96–−1.65	Cold spot	90% confidence level
−2.58–−1.96	Cold spot	95% confidence level
<−2.58	Cold spot	99% confidence level

The emerging hotspot analysis technique, available as a tool in the space–time pattern mining module of the Arc Pro software suite, was used to evaluate temporal evolution trends and characterize landslide clustering patterns. The spatial and temporal bins were set to  $5\text{ m} \times 5\text{ m}$  and 1 year, respectively, and the spatial and temporal search radii were set to 25 m and 5 years, respectively. The derived landslide clustering patterns were classified into 17 categories: 8 hotspot patterns, 8 cold spot patterns, and no pattern. The

8 hotspot and cold spot patterns were denoted as consecutive, diminishing, historical, intensifying, new, oscillating, persistent, and sporadic hotspots or cold spots, depending on the number of times the landslide bins were identified, the increases and decreases in landslide clustering intensity, and statistical significance (Table 2).

**Table 2.** The definition of spatiotemporal hotspot patterns by emerging hotspot analysis.

Pattern	Abbr. <sup>1</sup>	Definition
No pattern detected	—	A bin that did not fall into any of the hotspot or cold spot patterns defined below.
New hotspot (cold spot)	NHS (NCS)	A bin that was a statistically significant hotspot (cold spot) for the final year and had never been a statistically significant hotspot (cold spot) before.
Consecutive hotspot (cold spot)	CHS (CCS)	A bin with a single, uninterrupted run of statistically significant hotspot (cold spot) bins in the final year. The bin had never been a statistically significant hotspot (cold spot) prior to the final hotspot (cold spot) run, and less than 90% of all bins were statistically significant hotspots (cold spots).
Intensifying hotspot (cold spot)	IHS (ICS)	A bin that was a statistically significant hotspot (cold spot) for 90% of the year intervals, including the final year. In addition, the intensity of clustering of high counts in each year was increasing overall, and that increase was statistically significant.
Persistent hotspot (cold spot)	PHS (PCS)	A bin that was a statistically significant hotspot (cold spot) for 90% of the year intervals with no discernible trend indicating an increase or decrease in the intensity of clustering over time.
Diminishing hotspot (cold spot)	DHS (DCS)	A bin that was a statistically significant hotspot (cold spot) for 90% of the year intervals, including the final year. In addition, the intensity of clustering in each year was decreasing overall, and that decrease was statistically significant.
Sporadic hotspot (cold spot)	SHS (SCS)	A bin that was an on-again then off-again hot spot. Less than 90% of the year intervals were statistically significant hotspots (cold spot), and none of the year intervals were statistically significant cold spots (hotspots).
Oscillating hotspot (cold spot)	OHS (OCS)	A statistically significant hotspot (cold spot) for the final year that had a history of also being a statistically significant cold spot (hotspot) during a prior year. Less than 90% of the time-step intervals were statistically significant hotspots (cold spots).
Historical hotspot (cold spot)	HHS (HCS)	The most recent year was not hot (cold), but at least 90% of the year intervals were statistically significant hotspots (cold spots).

<sup>1</sup> Abbr. means the abbreviation for the pattern.

## 4. Results

### 4.1. Annual Rainfall and Landslide Records in 1999–2017

The annual rainfall data from the Jiasian and Singaokou stations were used to analyze the temporal changes in annual rainfall in the Chishan river watershed during 1999–2017. The rainfall characteristics of the Chishan river watershed during 1999–2017 are presented in Figure 4 and summarized in Table 3. At the Jiasian station, the average annual rainfall during 1999–2017 was higher than that during 1950–2020; moreover, at the Singaokou station, the average annual rainfall during 1999–2017 was higher than that during 1983–2020. The annual rainfall during 1999–2017 was higher than that during 1950–1998. The accumulated rainfall in the rainy season at the Jiasian station during 1999–2017 accounted for 92.2–93.8% of the average annual rainfall, and that at the Singaokou station accounted for 78.6–82.8%. Typhoon Morakot in 2009, a heavy-rainfall event with a return period of >200 years [7], was the strongest heavy-rainfall event during 1999–2017 in the Chishan

river watershed. This study compared the rainfall characteristics before and after Typhoon Morakot.

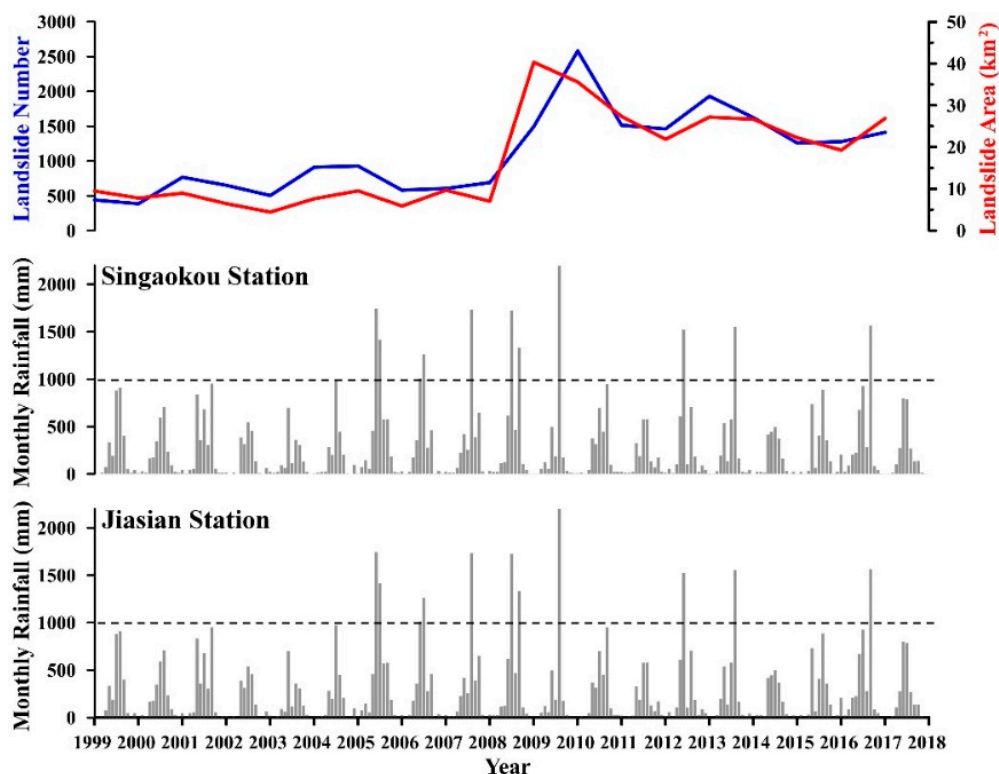


**Figure 4.** The distribution of monthly rainfall at the Jiasian (down plot) and Singaokou (middle plot) stations and the annual landslide number (blue line in upper plot) and area (red line in upper plot) during 1999–2017 in the Chishan river watershed.

**Table 3.** The rainfall characteristics at the Jiasian and Singaokou rainfall stations in 1999–2017 in the Chishan river watershed.

Time	Rainfall Characteristic	Jiasian	Singaokou
1999–2017	Average annual rainfall	3100 mm	3232 mm
	Average accumulated rainfall in rainy seasons	2886 mm	2683 mm
1999–2008	Average annual rainfall	3208 mm	3233 mm
	Average accumulated rainfall in rainy seasons	3010 mm	2678 mm
	Number of monthly rainfalls >1000 mm	7	6
	Number of daily rainfalls >652.8 mm <sup>1</sup>	1	1
2009–2017	Average annual rainfall	2980 mm	3423 mm
	Average accumulated rainfall in rainy seasons	2748 mm	2689 mm
	Number of monthly rainfalls >1000 mm	4	4
	Number of daily rainfalls >659.6 mm <sup>1</sup>	1	2

<sup>1</sup> The 652.8 mm and 659.6 mm measurements represent the daily rainfalls with return periods of 50 years at the Jiasian and Singaokou stations based on empirical equations from the regulations on soil and water conservation in Taiwan.

The accumulated rainfall in the rainy seasons, i.e., from May to October, and the number of monthly rainfalls >1000 mm at the Jiasian and Singaokou stations were used to describe the temporal distribution during 1999–2008 in the Chishan river watershed. The accumulated rainfall in the rainy seasons and the number of monthly rainfalls >1000 mm during 1999–2008 were greater than or close to those during 2009–2017. Using empirical equations provided in the regulations on soil and water conservation in Taiwan, this study estimated that the amounts of daily rainfall with return periods of 50 and 200 years were 601.3 and 704.3 mm, respectively, at the Jiasian rainfall station and 607.6 and 711.6 mm,

respectively, at the Singaokou rainfall station. During 1999–2017, the numbers of daily rainfall events in which the amount of rainfall exceeded 601.3 mm at the Jiasian station and 607.6 mm at the Singaokou station were two and three, respectively. The two events recorded at the Jiasian station were Typhoon Kalmaegi (629.5 mm on 17 July 2008) and Typhoon Morakot (1072.0 mm on 8 August 2009), and the three events recorded at the Singaokou station were Typhoon Kalmaegi (609.5 mm on 9 June 2005), Typhoon Morakot (833.0 mm on 8 August 2009), and Typhoon Morakot (780.0 mm on 9 August 2009). The rainfall characteristics in the Chishan river watershed during 1999–2017 featured plenty of rainfall with high rainfall intensity, concentrated in the rainy seasons. These results indicated that the strengths of rainfall-induced landslides during 1999–2008 in the Chishan river watershed were greater than those during 2009–2017, except for the landslides induced by Typhoon Morakot.

Data on the numbers and areas of landslides during 1999–2017 in the Chishan river watershed were used to explain temporal changes in landslides. The results revealed obvious differences between the numbers and areas of landslides before and after Typhoon Morakot. Analysis of landslide disaster data during 1999–2017 showed that the considerable number of landslide disasters during 2008–2017 was larger than that during 1999–2008. The numbers of landslides were 385–927 during 1999–2008, 1494 after Typhoon Morakot, and 1258–2581 during 2010–2017. The landslide areas were 4.4–9.7 km<sup>2</sup> during 1999–2008, 40.4 km<sup>2</sup> after Typhoon Morakot, and 19.2–35.6 km<sup>2</sup> during 2010–2017. The numbers and areas of landslides during 2010–2017 were 2.8–3.3 and 3.7–4.4 times higher, respectively, than those during 1999–2008. The obvious increases in the numbers and areas of landslides demonstrated the considerable impact of Typhoon Morakot on the landslide susceptibility of the Chishan river watershed.

The frequency of landslides [13] was defined as the total number of landslides occurring in each grid during 1999–2017, as shown in Figure 5. This information was used to explain the spatial changes in landslide susceptibility in the Chishan river watershed. Areas with a landslide frequency of 0 accounted for 91.0% of the study area, and those with a landslide frequency of >5 accounted for 3.0% of the area. Areas with a landslide frequency of >5 were concentrated along the rivers and in the sources of rivers in the C04–C10 subwatersheds, especially in the C07–C10 subwatersheds. These results indicated that the landslide distributions during 1999–2017 in the Chishan river watershed were related to the distribution of rivers. The landslide distributions in 1999, 2003, 2005, 2008, 2009, 2012, 2013, 2016, and 2017 in the Chishan river watershed are illustrated in Figure 4. Landslides were distributed in the C08–C10 subwatersheds before 2009 and then distributed densely in the C03–C10 subwatersheds after Typhoon Morakot. The landslide distribution narrowed, but it was still densely spread in the C04–C05 and C07–C10 subwatersheds during 2010–2017. The upstream subwatersheds, including C07–C10, were always susceptible to landslides, but the midstream subwatersheds, including C04–C05, became susceptible to landslides after Typhoon Morakot.

Rainfall events primarily triggered the evolution of large-earthquake-induced landslides [1,4], but they were not the only triggers for the evolution of extreme-rainfall-induced landslides [7,8]. According to the spatial and temporal distributions of landslides during 1999–2017, differences existed between the landslide distributions before and after Typhoon Morakot in the Chishan river watershed. Despite the decreasing strength and numbers of rainfall-induced landslides after Typhoon Morakot, the landslide area tended to decrease continuously, but the number of landslides tended to fluctuate in the Chishan river watershed. This fluctuation indicates that recovery from landslides was difficult and that landslides were easily reinduced.

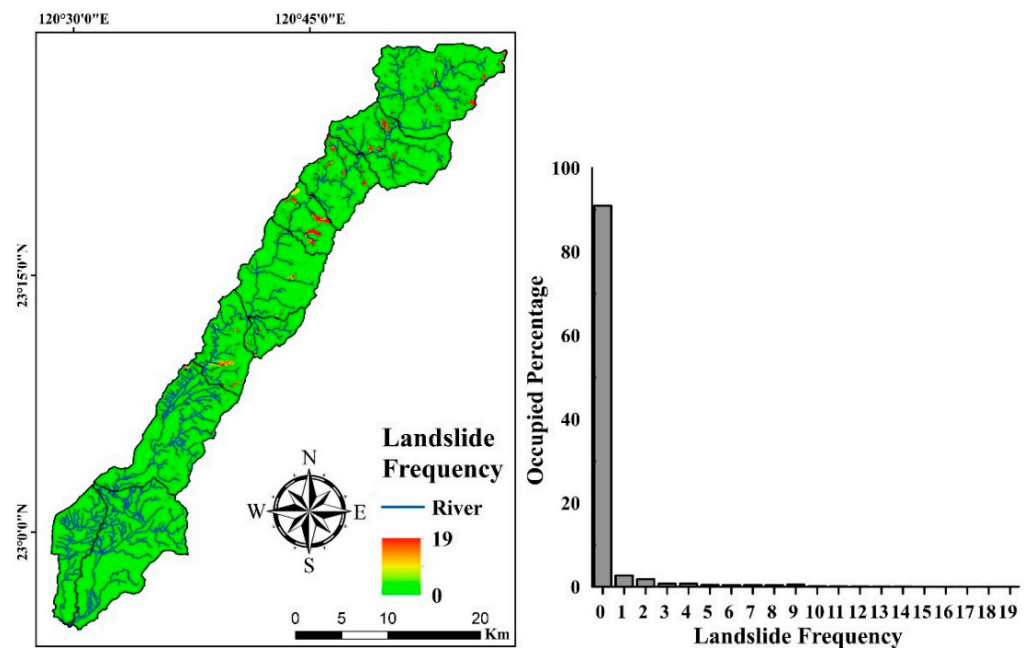


**Figure 5.** The distribution of landslide frequency from 1999 to 2017 in the Chishan river watershed.

#### 4.2. Certainty Factor Analyses of Landslide Occurrence in 1999–2017

This study applied a certainty factor to analyze the effectiveness of four geomorphologic factors—namely elevation, slope, aspect, and distance to rivers—at affecting the occurrence of landslides during 1999–2017 in the Chishan river watershed by using the landslide inventories of 1999, 2001, 2005, 2006, 2009, 2010, 2012, 2013, 2015, and 2017. Most of the landslides in the Chishan river watershed were induced by rainfall events. The analysis results obtained in the Chishan river watershed by using the certainty factor were compared with those obtained in other earthquake-induced landslide areas [6,31]. Figure 6 presents the relationships between landslide occurrence and the four geomorphologic factors.

Positive certainty factor values were derived in areas with elevations of >1000 m during 1999–2008. Moreover, the certainty factor values in areas with elevations of >2000 m increased with time. In 2009, positive certainty factor values were obtained in areas with elevations of 500–1750 m, but the certainty factor values in the areas with elevations of >2000 m were negative. The certainty values in areas with elevations of <1000, 1000–1750, and >1750 m decreased, were positive, and increased, respectively. In areas with elevations of >2000 m, recovery from landslides was difficult, and landslides were easily reinduced, as determined on the basis of the long-term distribution of certainty factor values with respect to elevation during 1999–2017. The areas in which recovery from landslides was difficult and in which landslides were easily reinduced were determined to be valuable for the analysis of landslide evolution. The elevations of these areas in the Chishan river watershed after Typhoon Morakot were similar to the elevations observed after the 2008 Wenchuan earthquake in Sichuan, China [6].

The areas with positive certainty factor values during 1999–2008, 2009, and 2010–2017 in the Chishan river watershed had slopes of >40°. The certainty factor values in these areas during 2010–2017 increased gradually. The certainty factor values were higher in areas with steeper slopes. In these areas, recovery from landslides was difficult, and landslides were easily reinduced, as determined on the basis of the long-term distribution of the certainty factor values with respect to slope during 1999–2017. The slopes in these areas in the Chishan river watershed after Typhoon Morakot were the same as those observed after the 2008 Wenchuan earthquake in Sichuan, China [6].

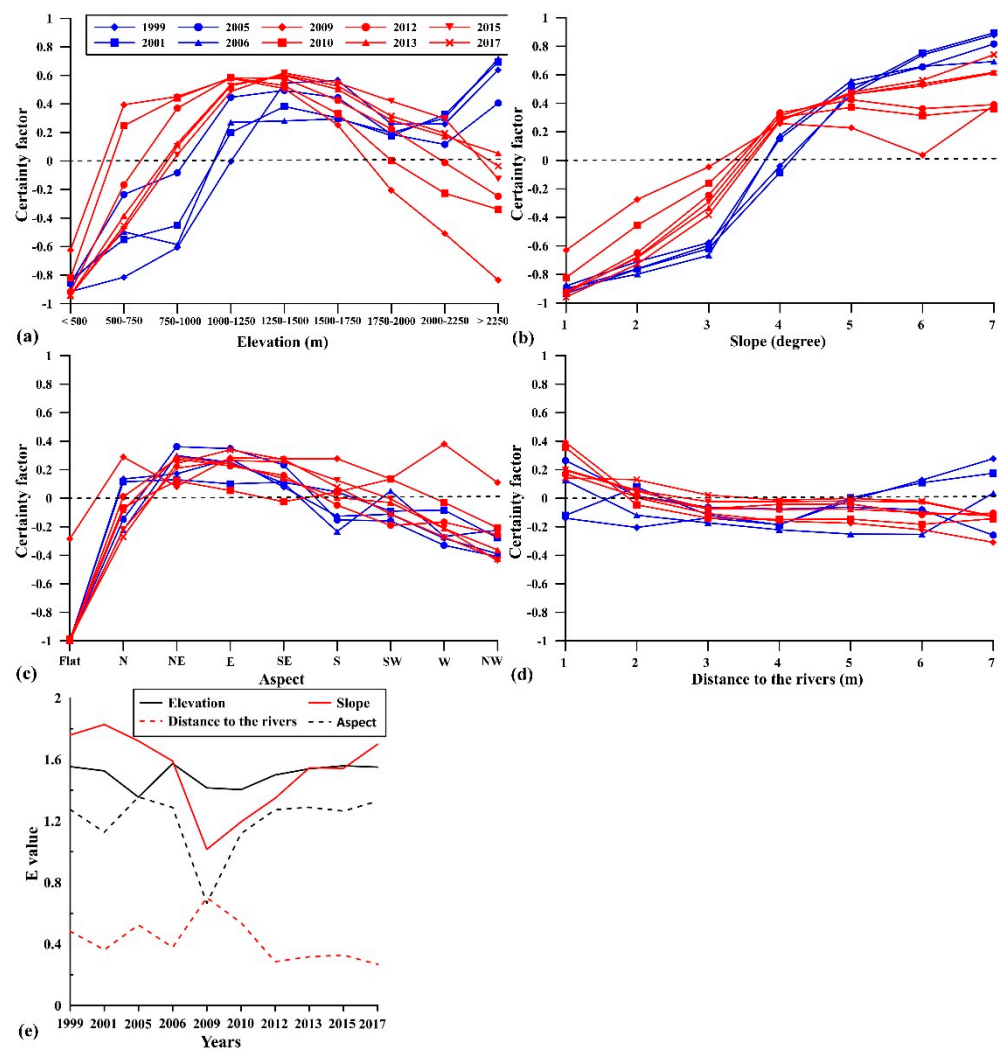


**Figure 6.** The certainty factor analysis in regard to elevation (a), slope (b), aspect (c), and distance to the rivers (d) and the *E* index values for these four factors (e) in the Chishan river watershed.

The slopes of the areas with positive certainty factor values during 1999–2008 had NE, E, and SE aspects. After Typhoon Morakot, the slopes of the areas with positive certainty factor values were in all aspects except for the flat aspect. Furthermore, the slopes of the areas with positive certainty factor values during 2009–2017 had N, NE, E, and SE aspects. In the Chishan river watershed, the slopes of the areas with high landslide susceptibility and difficulty recovering from landslides had N, NE, E, and SE aspects, as determined on the basis of the long-term distribution of certainty factor values with respect to aspect during 1999–2017. The aspects of slopes in the landslide-prone areas after large-earthquake-induced landslide events were similar to the directions of earthquake-causing faults [6], but the aspects of slopes in the landslide-prone areas in the Chishan river watershed after extreme-rainfall-induced landslide events were similar to windward side of the monsoon.

Studies have reported that the surroundings of rivers in upstream watersheds in Taiwan are susceptible to landslides [9,10]. This study revealed that the certainty factor values derived in areas within 400 m of rivers in the Chishan river watershed were negative after the 1999 Chichi earthquake event, indicating that the surroundings of rivers are not earthquake-induced landslide-prone areas. The certainty factor values derived in areas within 100 m of rivers were positive during 2005–2008. The certainty factor values reached their maximum during 1999–2017, 0.4, in areas within 100 m of rivers after Typhoon Morakot in the Chishan river watershed. The certainty factor values derived in areas within 100 m of rivers in the Chishan river watershed were greater than 0.15 during 2010–2017, and

those derived in areas within 100–200 m of rivers were positive during 2012–2017. These results indicated that in terms of long-term landslide evolution after extreme rainfall or large earthquake events, areas around rivers in the Chishan river watershed had difficulty recovering from landslides, and landslides were easily reinduced in these areas.

The effectiveness index ( $E$ ) was used to compare changes in the temporal effect of each factor on landslide occurrence during 1999–2017 in the Chishan river watershed (Figure 6e). The top two factors affecting landslide occurrence during 1999–2017 were elevation and slope, meaning that landslide location was a major factor affecting landslide evolution in the Chishan river watershed. Distance to rivers did not seem to have a clear effect on landslide evolution in the Chishan river watershed. Distance to rivers had the lowest effectiveness index ( $E$ ) among all four factors, and its effectiveness index decreased rapidly after Typhoon Morakot.

#### 4.3. Result of Local Outlier Analysis

The study conducted local outlier analysis to recognize the bins with landslide spatiotemporal statistical significance by using the local Anselin Moran's  $I$  index, and the statistical results are shown in Table 4. The multiple type dominated the spatiotemporal clustering pattern of landslide evolution during 1999–2008 and 2008–2017 in the Chishan river watershed. The areas of only high–high and low–low cluster patterns during 2008–2017 in the Chishan river watershed were obviously larger than those during 1999–2008. The distribution trend of the spatiotemporal clustering patterns of landslide evolution in the C10 subwatershed was similar to that in the Chishan river watershed. The distribution maps of local outlier analysis in the C10 subwatershed and Chishan river watershed are shown in Figure 7. The multiple types were widely spread in the C04 to C10 subwatersheds from 1999–2008 to 2008–2017. The only high–high clusters were recognized in the source areas of creeks and the neighborhoods of sinuous rivers, especially in the C10 subwatershed.

**Table 4.** The statistical results of local outlier analysis during 1999–2008 and 2008–2017 in the C10 subwatershed and the Chishan river watershed.

Patterns	Chishan River Watershed				C10 Subwatershed			
	1999–2008		2008–2017		1999–2008		2008–2017	
	A (ha) <sup>1</sup>	Per. <sup>1</sup>	A (ha)	Per.	A (ha)	Per.	A (ha)	Per.
Mul. <sup>1</sup>	1881.2	94.3	4073.7	83.7	703.0	94.8	798.3	83.1
NS. <sup>1</sup>	0.1	0.0	0.4	0.0	0.0	0.0	0.1	0.0
HH <sup>1</sup>	42.3	2.1	413.5	8.5	17.2	2.3	91.3	9.5
HL <sup>1</sup>	0.0	0.0	0.1	0.0	0.0	0.0	0.0	0.0
LH <sup>1</sup>	2.3	0.1	11.3	0.2	1.1	0.2	3.1	0.3
LL <sup>1</sup>	68.9	3.5	368.4	7.6	20.3	2.7	68.3	7.1

<sup>1</sup> Mul., NS., HH, HL, LH, and LL mean multiple types, never significant, only high–high cluster, only high–low cluster, only low–high cluster, and only low–low cluster, respectively. A and Per. mean area and percentage, respectively.

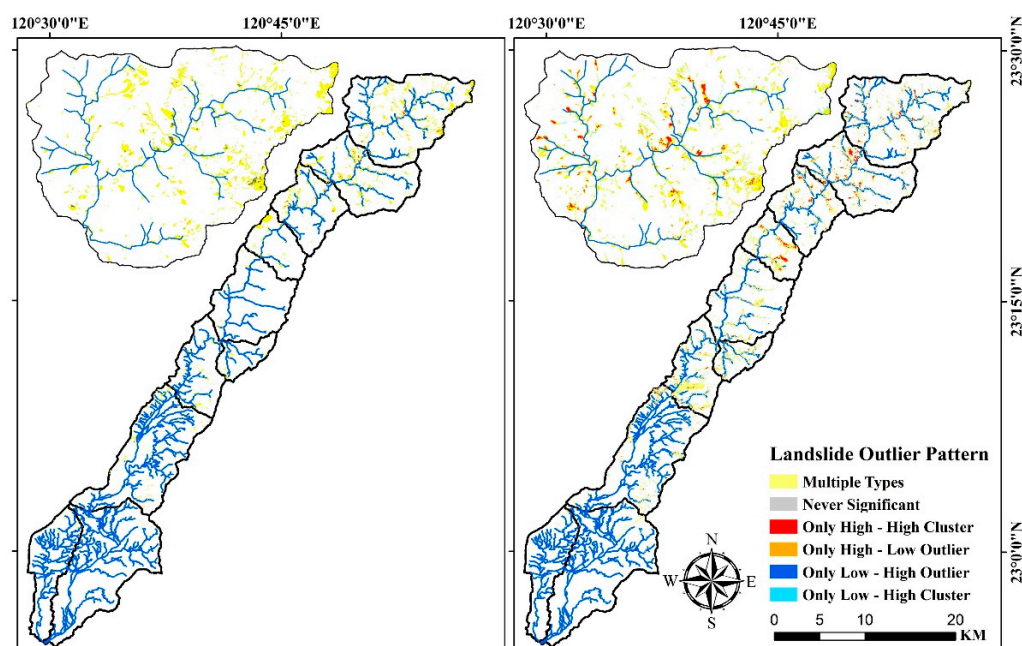


**Figure 7.** Local outlier analysis of landslide evolution during 1999–2008 (**left figure**) and 2008–2017 (**right figure**) in the Chishan river watershed.

#### 4.4. Spatiotemporal Hotspot Distribution

Emerging hotspot analysis was used to explore the spatiotemporal hotspot distribution and patterns of landslide evolution during 1999–2017 in the Chishan river watershed. Previous studies have not examined the evolution trends of landslide clustering before and after Typhoon Morakot in the Chishan river watershed. A spatiotemporal analysis can provide a comprehensive view of landslide clustering locations. Accordingly, the present study performed the Mann–Kendall trend test to demonstrate changes in the spatial clustering of landslides in each grid during 1999–2008 and 2008–2017 (Figure 6). The spatial clustering distributions of landslides in the Chishan river watershed during 1999–2008 (Figure 6a) and 2008–2017 (Figure 6b) were remarkably different; areas with increasing landslide occurrence trends are clearly highlighted in Figure 6. The numbers of grids with no significant trend, declining trends, and increasing trends during 2008–2017 were 1.1, 3.1, and 8.9 times larger, respectively, than those during 1999–2008. These results imply that the trends of landslide clustering in the Chishan river watershed after Typhoon Morakot were clearer than those after the 1999 Chichi earthquake.

Moreover, grids with increasing trends were concentrated in the upstream subwatersheds (C07–C10) during 2008–2017. The numbers of grids with no significant trend, declining trends, and increasing trends during 2008–2017 in the upstream subwatersheds were 0.89, 1.07, and 9.06 times larger, respectively, than those during 1999–2008. The number of grids with increasing trends in the upstream subwatersheds during 2008–2017 accounted for 82.6% of those in the Chishan river watershed, meaning that the upstream subwatersheds represented the main areas with landslide clustering in the Chishan river watershed during 2008–2017. The spatial distribution of landslide clustering in C10 is illustrated in Figure 8. The grids with increasing trends in C10 were clustered along the rivers, in the source areas of the rivers, and in the surroundings of large landslides. In Taiwan, the locations of landslides have been reported to be related to geomorphological factors and rainfall distribution during heavy rainfall events [1,7,8,12]. However, the present study revealed that river systems and large landslide cases influenced the locations where landslides were difficult to recover from and easy to reinduce in the upstream of the Chishan river watershed during 2008–2017.

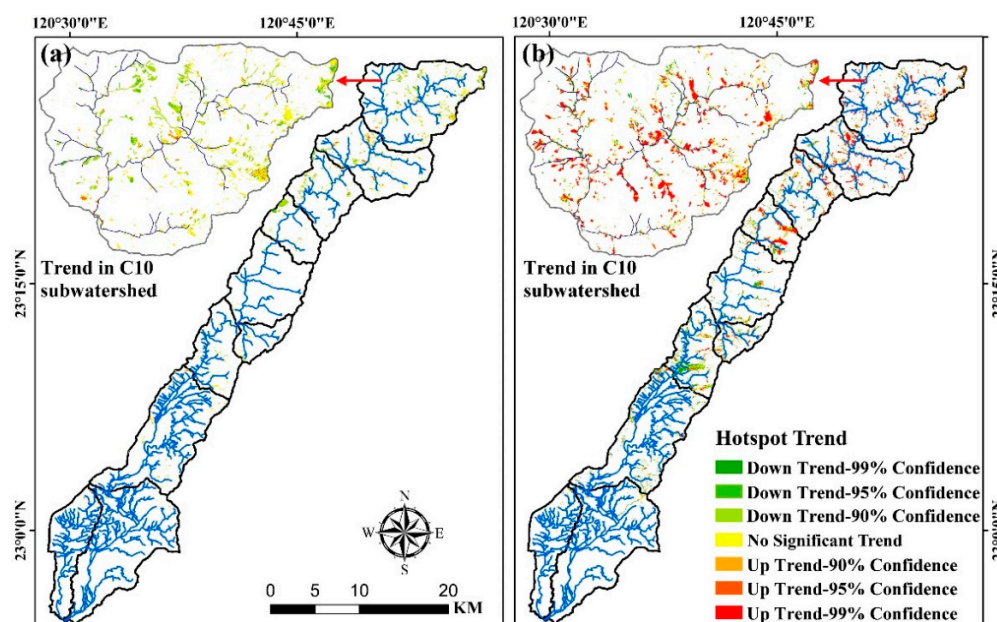


**Figure 8.** The spatial clustering distributions of landslides in 1999–2008 (a) and 2008–2017 (b) as assessed by using the Mann–Kendall trend test in the Chishan river watershed. The upper-left plots show the spatial clustering distribution of landslides in the C10 subwatershed in 1999–2008 (a) and 2008–2017 (b).

Figure 9 shows the differences in the spatiotemporal patterns and distributions of landslide hotspots during 1999–2008 and 2008–2017. The three main cold spot patterns during 1999–2008 were oscillating cold spots (OCS), persistent cold spots (PCS), and intensifying cold spots (ICS), and those during 2008–2017 were OCS, PCS, and sporadic cold spots (SCS). The three main hotspot patterns during 1999–2008 were oscillating hotspots (OHS), persistent hotspots (PHS), and intensifying hotspots (IHS), and those during 2008–2017 were OHS, HIS, and PHS. The characteristics of the main hotspot and cold spot patterns before and after Typhoon Morakot were oscillating and persistent, respectively.

During 1999–2017, the landslide hotspots were mainly distributed upstream of the Chishan river watershed. The main landslide hotspots in the upstream subwatersheds during 1999–2008 and 2008–2017 occupied 89.4% and 80.1%, respectively, of those in the Chishan river watershed. The main landslide hotspot in the upstream subwatersheds during 2008–2017 was 3.2 times larger than that during 1999–2008. OHS appeared in all upstream subwatersheds, but they were centralized in the surroundings of rivers and gullies and in the source areas of landslides. IHS and PHS were centralized in the core landslide areas and the downslopes of riverbank landslide areas.

The spatiotemporal patterns and distributions of the main landslide hotspots in the Chishan river watershed were related to the landslide area. The main landslide hotspot areas occupied 42.3%, 50.1%, and 59.1% of the large-, medium-, and small-landslide areas, respectively.

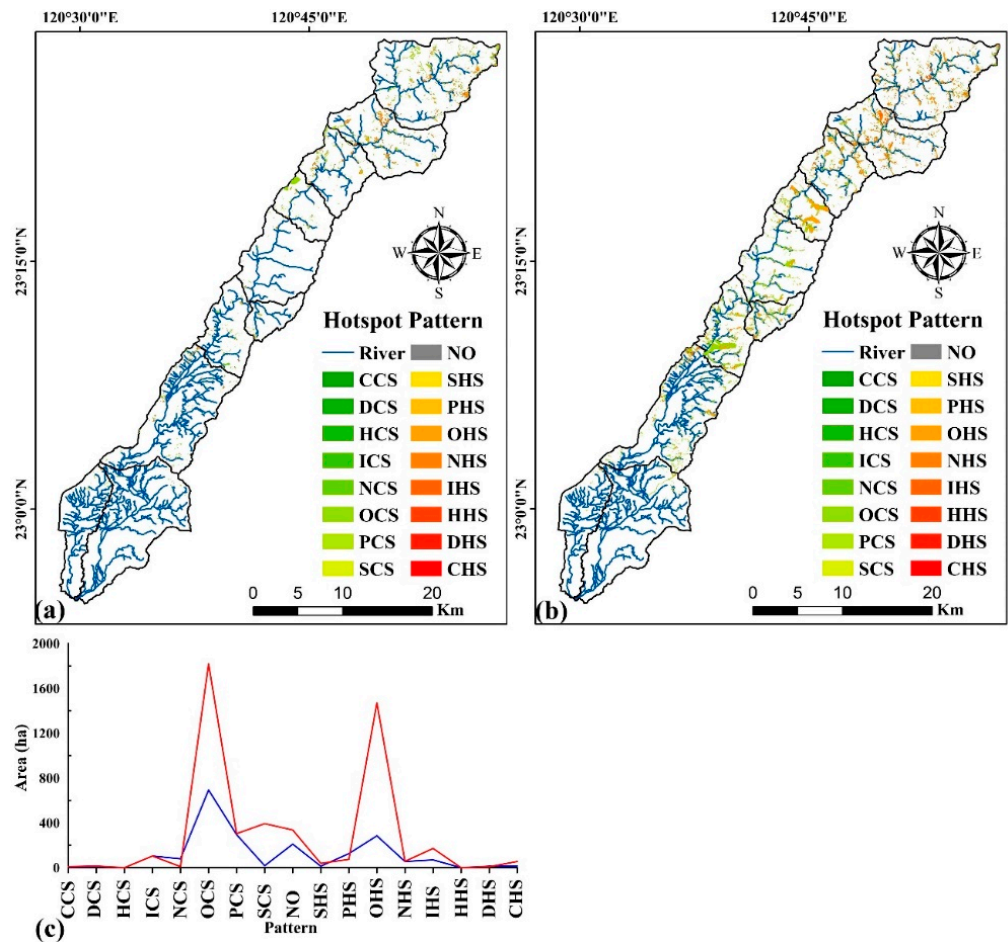


**Figure 9.** The patterns and distributions of landslide spatiotemporal hotspots in 1999~2008 (a) and 2008~2017 (b) in the Chishan river watershed. (c) shows the occupied percentage of each spatiotemporal hotspot pattern in 1999~2008 (blue line) and 2008~2017 (red line).

#### 4.5. Clustering Strength of Small, Medium, and Large Landslides

In the Getis–Ord formula for hotspot analysis, the Z-score indicates the statistical significance of hotspots and cold spots; this study used it as an index to assess the strength of landslide clustering and estimate oscillation periods. A higher Z-score was considered to indicate more obvious landslide clustering, with a Z-score of 0 or a negative Z-score indicating the absence of landslide clustering. Figure 10 presents the average Z-scores during 1999–2008 and 2008–2017 in the Chishan river watershed.

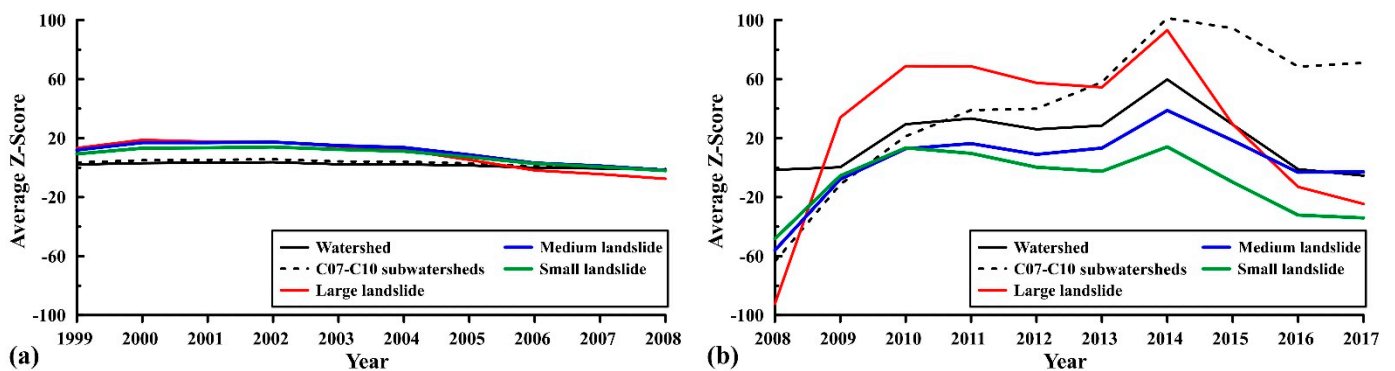


**Figure 10.** Temporal distribution of average Z-scores in the Chishan river watershed (black line), upstream subwatersheds (C07–C10, black dash line), large landslide cases (red line), medium landslide cases (blue line), and small landslide cases (green line) in 1999–2008 (a) and 2008–2017 (b).

The temporal distributions of the clustering strengths of large, medium, and small landslides during 1999–2008 were similar, and those of landslides during 2008–2017 were also similar. During 1999–2004, the landslides could be ordered as follows in terms of strength (in decreasing order): large, medium, and small landslides. Moreover, during 2005–2008, they could be ordered as follows in terms of strength (in decreasing order): medium, small, and large landslides. These results demonstrate that the clustering strength of large landslides in the Chishan river watershed was high only in the early years after the 1999 Chichi earthquake.

The distributions of the clustering strength of the large, medium, and small landslides during 2010–2014 fluctuated, and the strength decreased rapidly from 2015 onward. The clustering of small landslides induced by Typhoon Morakot was not obvious, and the average Z-score derived for small landslides was positive only during 2010–2012 and in 2014. The average Z-scores derived for large and medium landslides induced by Typhoon Morakot were positive in the subsequent 5 years, and they started to decrease rapidly from 2015 onward.

## 5. Discussion

The spatiotemporal hotspots and cold spots of landslides can indicate the clustering strength of landslides and the patterns of landslide locations. Moreover, the spatiotemporal distribution of landslide hotspots is directly related to the evolution and recovery of a watershed after extreme-rainfall-induced landslide events, and it exerts a strong negative effect on the sustainability of watershed management. The oscillation period [9] can be defined as the period during which the number or area of landslides fluctuates in the years that follow severe landslide events. The oscillation period can also be defined as the time needed for the watershed to stably recover from landslides. Landslide evolution research has used different methods to assess landslide recovery time and the oscillation period after large-earthquake- and extreme-rainfall-induced serious landslide events. The spatial distribution of landslide recovery has been assessed by estimating the landslide activity, and the temporal changes in landslide recovery have been assessed by observing the numbers and areas of landslides every year after serious landslide events, after the 2005 Kashmir earthquake [2] and the 2008 Wenchuan earthquake [4–6]. The oscillation period was estimated to be 3–5 years after the 2005 Kashmir earthquake and the 2008 Wenchuan earthquake and 5 years after Typhoon Morakot in southern Taiwan [9].

The 1999 Chichi earthquake induced 439 landslide cases covering a total area of 9.5 km<sup>2</sup> in the Chishan river watershed. The average Z-score in the Chishan river watershed (Figure 10) was 2.15 in 1999; it increased to 3.04–3.68 in 2000–2002 and then started to decrease in 2003 before finally dropping to –1.48 in 2008. Typhoon Morakot in 2009 induced 1494 landslide cases covering a total area of 40.3 km<sup>2</sup> in the Chishan river watershed. The average Z-score in the Chishan river watershed was 0.31 in 2009; it increased rapidly to 29.43 in 2010 and fluctuated between 26.02 and 29.78 during 2010–2014, after which it started to decrease in 2015 until reaching –5.37 in 2017. The average Z-score after the 1999 Chichi earthquake in the Chishan river watershed was 1.41 times greater than that before 1999, and the average Z-score after Typhoon Morakot was 94.94 times greater than that before 2009. These results demonstrate that the clustering strength of landslides induced by Typhoon Morakot in the Chishan river watershed was considerably greater than that of landslides induced by the 1999 Chichi earthquake. According to the temporal changes in the average Z-scores, the Chishan river watershed required 2 years to achieve stable recovery after the 1999 Chichi earthquake but 4 years after Typhoon Morakot. Accordingly, the oscillation period after Typhoon Morakot in the Chishan river watershed was twice as long as that after the 1999 Chichi earthquake. The results also indicated that recovery from landslides induced by a large earthquake ( $M_L = 7.3$ ) in Taiwan was faster than from those induced by an extreme rainfall event with accumulated rainfall of >2000 mm.

The average Z-scores in the upstream subwatersheds during 1999–2008 ranged from –0.95 to 5.66, and they were marginally higher than those in the Chishan river watershed.

However, the average Z-scores in the upstream subwatersheds during 2008–2017 ranged from  $-63.70$  to  $101.38$ , and those after 2010 were higher than those in the Chishan river watershed. The average Z-score in the upstream subwatersheds during 2016–2017 was approximately  $70.0$ , and that in the other area of the Chishan river watershed was negative. These results indicate that the landslide recovery period in the upstream subwatersheds was longer than that in the Chishan river watershed.

The spatial resolution of images that were used to identify the landslide was the major factor for the number of identified small landslides. The images used to identify landslides were Spot 1 and Spot 2 images with spatial resolution of  $10\text{ m}$  during 1999–2002 and Formosat-2 images with spatial resolution of  $2\text{ m}$  during 2003–2017. The number of small landslides ranged from 238 to 550 during 1999–2002, from 503 to 604 during 2003–2008, and from 1411 to 1930 during 2009–2017. The number of small landslides in the Chishan river watershed increased obviously after 2003, especially after Typhoon Morakot in 2009.

The number of small landslides was also the major reason explaining the temporal changes in Z-values. The number of small landslides was  $54.2$  to  $71.8\%$  of the total number of landslides during 1999–2002 and  $70.2$  to  $80.4\%$  during 2003–2017. The number of small landslide was 1494 in 2009, peaked at 1930 in 2014, and ended at 1411 in 2017. The fluctuation in the number of small landslides was similar to the temporal change in Z-values during 2009–2017. We suggest that the number of small landslides was the major factor for the average Z-value and that the location of medium and large landslides was the major factor for the distribution and patterns of spatiotemporal landslide hotspots based on the results on long-term landslide evolution in the Chishan river watershed.

The Z-values in the study provided quantified data on landslide clustering at different scales (watershed or subwatershed) and different landslide sizes (small, medium, and large) in different time periods. Using Z-values to explain the spatial distribution of and temporal changes in landslide recovery can be a convincing method for explaining landslide evolution.

Using spatiotemporal hotspot analysis to analyze landslide evolution in the study provided powerful theoretical evidence to explain the spatial and temporal distribution of landslide clustering. The patterns and distributions of landslide spatiotemporal hotspots can also explain the characteristics of watershed recovery after serious landslide events and can thus represent useful information for formulating policies for watershed recovery.

## 6. Conclusions

We analyzed the effectiveness of landslide occurrence and recovery and explained the patterns and distributions of landslide hotspots in the Chishan river watershed during 1999–2017. The numbers and areas of landslides in the Chishan river watershed after Typhoon Morakot in 2009 were around three times larger than those after the 1999 Chichi earthquake, and this result indicated that the impact of Typhoon Morakot on the landslide susceptibility in the Chishan river watershed was stronger and more obvious than that of the 1999 Chichi earthquake. We evaluated the effectiveness of landslide occurrence and recovery during 1999–2017 by using a certainty factor and compared the importance of four geomorphologic factors affecting the landslide occurrence. The concentration of landslide occurrence and evolution in the Chishan river watershed was more related to the factors of elevation and slope than to those of aspect and distance to the river. We built a spatiotemporal cube model by using the annual landslide inventories during 1999–2017 and explained the spatiotemporal characteristics of landslide hotspots by using emerging hotspot analysis. The main hotspot patterns in the Chishan river watershed were OHS, PHS, and IHS, while the main cold spot patterns were OCS, PCS, and SCS. We explained the temporal changes in landslide clustering by using the Z-score and found that the core landslide areas and the downslopes of riverbank landslide areas in the upstream of the Chishan river watershed were the areas of highest landslide susceptibility. The long-term monitoring of landslide occurrence and recovery is useful for understanding the recovery time after landslides and temporal changes in landslide susceptibility. The findings on the

evolution of postearthquake and post-extreme rainfall landslides in this study are valuable for the prediction and disaster prevention of future geohazards.

**Funding:** This research was funded by Project Research in Feng Chia University (number: 20H00710 and 21H00710).

**Institutional Review Board Statement:** Not applicable.

**Informed Consent Statement:** Not applicable.

**Data Availability Statement:** Not applicable.

**Conflicts of Interest:** The author declares no conflict of interest.

## References

1. Lin, C.W.; Liu, S.H.; Lee, S.Y.; Liu, C.C. Impacts of the Chi-Chi earthquake on subsequent rainfall-induced landslides in Central Taiwan. *Eng. Geol.* **2006**, *86*, 87–101. [[CrossRef](#)]
2. Shafique, M. Spatial and temporal evolution of co-seismic landslides after the 2005 Kashmir earthquake. *Geomorphology* **2020**, *362*, 107228. [[CrossRef](#)]
3. Saba, S.B.; van der Meijde, M.; van der Werff, H. Spatiotemporal landslide detection for the 2005 Kashmir earthquake region. *Geomorphology* **2010**, *124*, 17–25. [[CrossRef](#)]
4. Yang, W.; Qi, W.; Wang, M.; Zhang, J.; Zhang, Y. Spatial and temporal analyses of post-seismic landslide changes near the epicentre of the Wenchuan earthquake. *Geomorphology* **2017**, *276*, 8–15. [[CrossRef](#)]
5. Li, C.; Wang, M.; Liu, K. A decadal evolution of landslides and debris flows after the Wenchuan earthquake. *Geomorphology* **2018**, *323*, 1–12. [[CrossRef](#)]
6. Chen, M.; Tang, C.; Xiong, J.; Shi, Q.Y.; Li, N.; Gong, L.F.; Wang, X.D.; Tie, Y. The long-term evolution of landslide activity near the epicentral area of the 2008 Wenchuan earthquake in China. *Geomorphology* **2020**, *367*, 107317. [[CrossRef](#)]
7. Wu, C.H.; Chen, S.C.; Chou, H.T. Geomorphologic Characteristics of Catastrophic Landslides during Typhoon Morakot in the Kaoping Watershed, Taiwan. *Eng. Geol.* **2011**, *123*, 13–21. [[CrossRef](#)]
8. Wu, C.H.; Chen, S.C.; Feng, Z.Y. Formation, failure, and consequences of the Xiaolin landslide dam, triggered by extreme rainfall from Typhoon Morakot, Taiwan. *Landslides* **2014**, *11*, 357–367. [[CrossRef](#)]
9. Rosser, N.; Kinsey, M.; Oven, K.; Densmore, A.; Robinson, T.; Pujara, D.S.; Shrestha, R.; Smutny, J.; Gurung, K.; Lama, S.; et al. Changing significance of landslide Hazard and risk after the 2015 Mw 7.8 Gorkha, Nepal Earthquake. *Prog. Disaster Sci.* **2021**, *10*, 100159. [[CrossRef](#)]
10. Chen, X.L.; Shan, X.J.; Wang, M.M.; Liu, C.G.; Han, N.N. Distribution Pattern of Coseismic Landslides Triggered by the 2017 Jiuzhaigou Ms 7.0 Earthquake of China: Control of Seismic Landslide Susceptibility. *ISPRS Int. J. Geo-Inf.* **2020**, *9*, 198. [[CrossRef](#)]
11. Huang, R.; Fan, X. The landslide story. *Nat. Geosci.* **2013**, *6*, 325–326. [[CrossRef](#)]
12. Wu, C.; Lin, C. Spatiotemporal hotspots and decadal evolution of extreme rainfall-induced landslides: Case studies in southern Taiwan. *Water* **2021**, *13*, 2090. [[CrossRef](#)]
13. Wu, C.H. Evaluating the landslide stability and vegetation recovery: Case studies in the Tsengwen reservoir watershed in Taiwan. *Water* **2021**, *13*, 3479. [[CrossRef](#)]
14. Zhang, S.; Zhang, L.M.; Glade, T. Characteristics of earthquake- and rain-induced landslides near the epicenter of Wenchuan earthquake. *Eng. Geol.* **2014**, *175*, 58–73. [[CrossRef](#)]
15. De Cos, O.; Castillo, V.; Cantarero, D. Differencing the risk of reiterative spatial incidence of COVID-19 using space–time 3D bins of Geocoded Daily Cases. *ISPRS Int. J. Geo-Inf.* **2021**, *10*, 261. [[CrossRef](#)]
16. Purwanto, P.; Utaya, S.; Handoyo, B.; Bachri, S.; Astuti, I.S.; Utomo, K.S.B.; Aldianto, Y.E. Spatiotemporal analysis of COVID-19 spread with emerging hotspot analysis and space–time cube models in east Java, Indonesia. *ISPRS Int. J. Geo-Inf.* **2021**, *10*, 133. [[CrossRef](#)]
17. Syetiawan, A.; Harimurti, M.; Prihanto, Y. A spatiotemporal analysis of COVID-19 transmission in Jakarta, Indonesia for pandemic decision support. *Geospat. Health* **2022**, *17*, 1042. [[CrossRef](#)]
18. Everett, B.I.; Fennessy, S.T.; van den Heever, N. Using hotspot analysis to track changes in the crustacean fishery off KwaZulu-Natal, South Africa. *Reg. Stud. Mar. Sci.* **2021**, *41*, 101553. [[CrossRef](#)]
19. Kang, Y.; Cho, N.; Son, S. Spatiotemporal characteristics of elderly population’s traffic accidents in Seoul using space-time cube and space-time kernel density estimation. *PLoS ONE* **2018**, *13*, e0196845. [[CrossRef](#)]
20. Cheng, Z.; Zu, Z.; Lu, J. Traffic crash evolution characteristic analysis and spatiotemporal hotspot identification of urban road intersections. *Sustainability* **2019**, *11*, 160. [[CrossRef](#)]
21. Cheng, S.; Zhang, B.; Peng, P.; Yang, Z.; Lu, F. Spatiotemporal evolution pattern detection for heavy-duty diesel truck emissions using trajectory mining: A case study of Tianjin, China. *J. Clean. Prod.* **2020**, *244*, 118654. [[CrossRef](#)]
22. Zhang, X.; Yao, J.; Sila-Nowicka, K.; Jin, Y. Urban Fire Dynamics and Its Association with Urban Growth: Evidence from Nanjing, China. *ISPRS Int. J. Geo-Inf.* **2020**, *9*, 218. [[CrossRef](#)]

23. Wu, C.H. Landslide susceptibility based on extreme rainfall-induced landslide inventories and the following landslide evolution. *Water* **2019**, *11*, 2609. [[CrossRef](#)]
24. Yang, S.Y.; Jan, C.D.; Wang, J.S. Landslides Triggered by Typhoon Morakot in Taiwan. In *Environmental Risks*, 1st ed.; Mihai, F.C., Grozavu, A., Eds.; Intech Open: London, UK, 2018; pp. 13–43.
25. Liu, C.C.; Liu, J.G.; Lin, C.W.; Wu, A.M.; Liu, S.H.; Shieh, C.L. Image processing of formosat-2 data for monitoring south asia tsunami. *Int. J. Remote Sens.* **2007**, *28*, 3093–3111. [[CrossRef](#)]
26. Liu, C.C.; Chen, P.L. Automatic extraction of ground control regions and orthorectification of formosat-2 imagery. *Opt. Express* **2009**, *17*, 7970–7984. [[CrossRef](#)]
27. Liu, C.C.; Shieh, C.L.; Wu, C.A.; Shieh, M.L. Change detection of gravel mining on riverbeds from the multi-temporal and high-spatial-resolution formosat-2 imagery. *River Res. Appl.* **2009**, *25*, 1136–1152. [[CrossRef](#)]
28. Liu, C.C.; Ko, M.H.; Wen, H.L.; Fu, K.L.; Chang, S.T. Instability Index Derived from a Landslide Inventory for Watershed Stability Assessment and Mapping. *ISPRS Int. J. Geo-Inf.* **2019**, *8*, 145. [[CrossRef](#)]
29. Shortliffe, E.H.; Buchanan, B.G. A model of inexact reasoning in medicine. *Math. Biosci.* **1975**, *23*, 351–379.
30. Heckerman, D. Probabilistic interpretations for Mycin's certainty factors. *Mach. Intell. Patt. Rec* **1986**, *4*, 167–196.
31. Xu, C.; Dai, F.C.; Yao, X.; Chen, J.; Tu, X.B.; Cao, Y.B.; Xiao, J.Z. GIS based certainty factor analysis of landslide triggering factors in Wenchuan earthquake. *Chin. J. Rock Mech. Eng.* **2010**, *29*, P2972–P2981. (In Chinese)
32. Lan, H.X.; Zhou, C.H.; Wang, L.J.; Zhang, H.Y.; Li, R.H. Landslide hazard spatial analysis and prediction using GIS in the Xiaojiang watershed, Yunnan, China. *Eng. Geol.* **2004**, *76*, 109–128. [[CrossRef](#)]
33. Anselin, L. Local Indicators of Spatial Association—LISA. *Geogr. Anal.* **1995**, *27*, 93–115. [[CrossRef](#)]
34. Ord, J.K.; Getis, A. Local spatial autocorrelation statistics: Distributional issues and an application. *Geogr. Anal.* **1995**, *27*, 286–306. [[CrossRef](#)]